Laser cooling and trapping of barium

De, Subhadeep

Chapter 4

Experimental Tools

The main experimental topic of this work is the optical trapping of the heavy alkaline-earth element barium as a precursor for radium experiments. Trapping of atoms in a magneto-optical trap (MOT) requires an atomic source inside a vacuum chamber, coherent light sources for driving suitable atomic transitions, a quadrupole magnetic field, a detector for observing the signal from trapped atoms and a data acquisition system. The experiments require the control of up to eight different lasers at the same time.

4.1 Barium Atomic Beam

A barium atomic beam is produced by a resistively heated effusive oven [112]. The same basic oven design is used for several experiments at KVI: as an atom source in the Alcatraz experiment aiming for trapping of the rare isotope ^{41}Ca [154] and as a source for Na trapping for recoil ion momentum spectroscopy [155, 156]. The oven is mounted on a standard CF35 flange. It is inserted into a CF35 tube of 128 mm length. An electric power of some 20 W heats the oven to a temperature of 820 K. The temperature can be measured with a K-type thermocouple, which is a model K24-1-505 (from KURVAL BV., Nieuw-Vennep, Netherlands). The oven crucible has an orifice of 1 mm diameter and 10 mm length. The divergence of the atomic beam is about 100 mrad. Far away from the oven, near the beam axis where the transverse velocity component can be neglected, the velocity distribution of the atoms in the atomic beam can be approximated with a Maxwell-Boltzmann distribution

$$\mathrm{dF_{beam}(v)} = \frac{\mathrm{v}^3}{2\,\widetilde{\mathrm{v}}^4}\,\exp\left(-\frac{\mathrm{v}^2}{2\,\widetilde{\mathrm{v}}^2}\right)\,\mathrm{dv}, \tag{4.1}$$

where v is the atomic velocity, m is the mass of a barium atom, k_B is Boltzmann's constant, T is the operating temperature of the oven and $\widetilde{v}$ is the characteristic velocity given by

$$\widetilde{v} = \sqrt{\frac{k_B \cdot T}{m}}. \tag{4.2}$$

In an atomic beam the average velocity is $< v >= \sqrt{\frac{9\pi}{8}} \cdot \widetilde{v}$, the most probable velocity is $v_{mp} = \sqrt{3} \cdot \widetilde{v}$ and the root-mean-square velocity is $v_{rms} = 2 \cdot \widetilde{v}$. In this distribution, a fraction of only $4 \cdot 10^{-5}$ is below a velocity of 30 m/s, a typical capture velocity of a MOT.

The oven is loaded with 200 mg of barium carbonate $BaCO_3$ and 500 mg zirconium Zr powder. The $BaCO_3$ is mixed with the Zr powder. The oven is heated initially to a temperature of 1000 K, to break the carbonate bond and to produce barium oxide BaO and carbon-di-oxide CO_2 in a calcination process. Zirconium works as a reducing agent for BaO to produce atomic Ba. Aluminum and silicon could be used as an alternative reducing agent in a thermite process. The flux is about $10^{12} - 10^{14}$ barium atoms per second emerging from the oven at a temperature range of $750 - 900$ K. Two identical ovens are operated in the experiment, one is filled with $BaCO_3$ (from ACROS Organics, NJ, USA), with the seven stable natural barium isotopes. The second oven contains isotopically enriched $^{138}BaCO_3$ of 99.7% purity (from Campro Scientific BV, Veenendaal, Netherlands).

The beam with all natural barium isotopes is used for Doppler free laser spectroscopy with the transition at wavelength λ_1. The obtained signal serves as a reference for stabilizing the laser frequency [112]. The isotopically pure ^{138}Ba atomic beam is used in the magneto-optical trapping setup.

The vacuum chambers for both atomic beams are made of standard conflat (CF) UHV stainless steel parts. The vacuum system for the Ba atomic beam consists of the oven in a CF63 chamber and CF38 triplecross piece. To this housing two windows are mounted on opposite sides for a laser beam entry and exit, which crosses the atomic beam at right angle $\theta = 90^o$ downstream of the oven. The interaction region can be viewed through a third window, which is orthogonal to the laser and atomic beams. The vacuum is maintained in this chamber by a 2 l/s ion pump (from Gamma Vacuum, MN, USA) to several times 10^{-9} mbar. The isotopically pure ^{138}Ba beam is connected to a vacuum system (see Fig. 4.1), which is pumped by a 10 l/s ion pump (from Gamma Vacuum, MN, USA). The vacuum is typically around 10^{-9} mbar. An octagon (from Kimball Physics Inc., NH, USA) is used as the central trapping chamber. It has ports

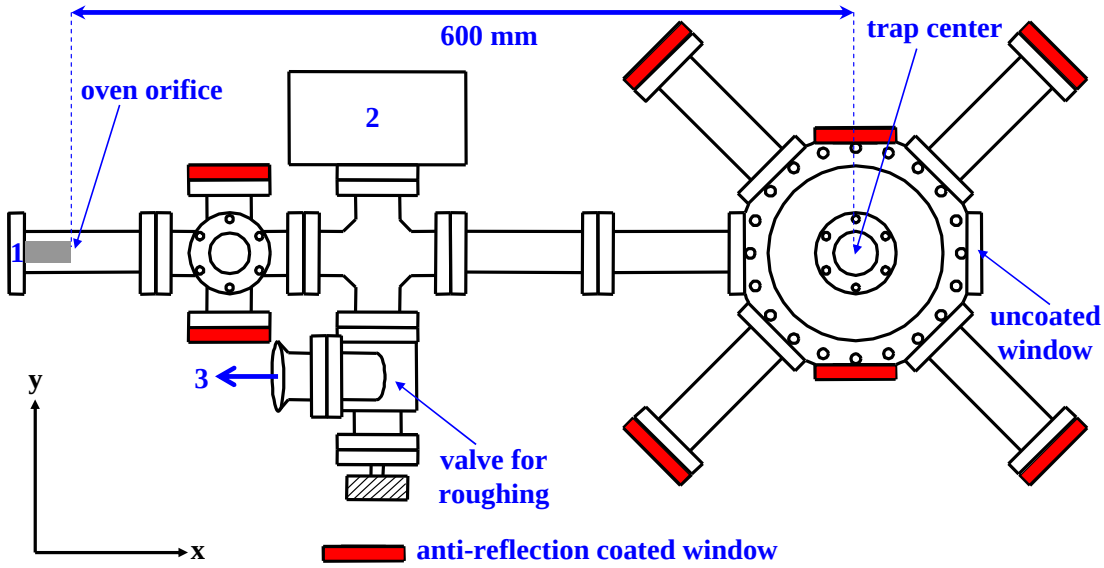

Fig. 4.1: Top view of the vacuum chamber for magneto-optical trapping of barium. 1 - the barium oven is mounted on a CF35 flange. 2 - a 10 l/s ion pump to maintain the vacuum. 3 - a KF port for mounting a roughing pump to the chamber. The optical windows indicated in bold are anti-reflection coated. The center of the octagon shaped part of the chamber is about 600 mm down stream of the oven orifice. Figure is drawn to scale.

for nine optical windows. Eight of the windows are made from fused silica and have a broad band anti-reflection coating to reduce the reflectivity at wavelength λ_1 to less than 0.5%. Some of the windows are mounted on extension tubes to reduce the amount of reflected stray light coming from six trapping laser beams. The window in the direction of the atomic beam has no optical coating, since it is used for several significantly different wavelengths.

4.2 Lasers

Lasers at visible and infrared wavelengths are needed for driving transitions in the laser cooling cycle (see Fig. 4.1). Different types of lasers are employed, i.e., a dye laser, three fiber lasers and several diode lasers. The laser systems, the generation of multiple frequencies at one wavelength, locking schemes and the layout of the optics arrangement are described in this section.

Wavelength (nm)	Transition	Intensity	Detuning	Laser system
$\lambda_1 = 553.7$	$6s^2\ {}^1S_0 \rightarrow 6s6p\ {}^1P_1$	I_1^p	$\Delta\nu_1^p$	Dye laser
$\lambda_2 = 659.7$	$6s5d\ {}^3D_1 \rightarrow 5d6p\ {}^3D_1^o$	I_2	$\Delta\nu_2$	Diode laser
$\lambda_3 = 667.7$	$6s5d\ {}^3D_2 \rightarrow 5d6p\ {}^3D_1^o$	I_3	$\Delta\nu_3$	Diode laser
$\lambda_{IR1} = 1107.8$	$6s5d\ {}^3D_1 \rightarrow 6s6p\ {}^1P_1$	I_{IR1}	$\Delta\nu_{IR1}$	Fiber laser
$\lambda_{IR2} = 1130.6$	$6s5d\ {}^3D_2 \rightarrow 6s6p\ {}^1P_1$	I_{IR2}^p	$\Delta\nu_{IR2}^p$	Fiber and diode lasers
$\lambda_{IR3} = 1500.4$	$6s5d\ {}^1D_2 \rightarrow 6s6p\ {}^1P_1$	I_{IR3}^p	$\Delta\nu_{IR3}^p$	Fiber and diode lasers

Table 4.1: Nomenclature for the intensities and frequency detunings of all laser beams in this work. Laser beams at the wavelengths λ_1, λ_{IR2} and λ_{IR3} are used for two different purposes in the experiments. For those lasers the superscript p (i.e. s or t) in the detunings and intensities refers to their purpose. Where s means slowing and t means trapping.

Dye Laser

A CR-699-21 ring dye laser (from Coherent Inc., Palo Alto, USA) is operated with Pyrromethene-567 (PM567) dye to produce light at wavelength λ_1. The concentration of the dye solution is 1 g in 1.5 ℓ of 2-phenoxyethanol (CAS No. 122-99-6). A dye circulator RD-2000 and a nozzle RD-07 (from Radiant Dyes Laser & Accessories GmbH, Wermelskirchen, Germany) are installed to the dye laser. The laser is pumped by a Verdi-V10 single frequency Nd:YAG laser (from Coherent Inc., Palo Alto, USA). The wavelength of this laser is 532 nm and it has a maximum output power of 10 W. Typically an ample amount of $420 - 440$ mW output power is generated by the dye laser at wavelength λ_1 with 5 W of pump power and 7.5 bar pressure in the dye circulator. The lasing threshold of the dye laser is reached for 2.8 W of pump power. The linewidth of the light is about 1 MHz. The dye laser frequency can be scanned over a range of 20 GHz, either internally or by an external control voltage.

Fiber Lasers

Three custom made fiber lasers (from Koheras Adjustik and Boostik Systems, Birkerød, Denmark) are used for generating light at the infrared wavelengths λ_{IR1}, λ_{IR2} and λ_{IR3}. The maximum output powers are 5 mW, 40 mW and 77 mW

Diode lasers				
Part No.	QLD-660 -80S	DL3149- 057	LD-1120 -0300-1	QFBLD -1550-20
Supplier	QPhotonics USA	Thorlabs USA	TOPTICA Germany	QPhotonics USA
Wavelength	λ_2	λ_3	λ_{IR2}	λ_{IR3}
Power (mW)	8	5	300	17
Typical frequency tuning coefficients				
Current (MHz/A)	1200	1000	175	10^6
Tuning Actuator	560 MHz/V (PZT)	500 MHz/V (PZT)	70 MHz/V (PZT)	21 MHz/Ω (thermistor)

Table 4.2: Characteristics of the diode lasers used in the experiments.

respectively. These lasers are tunable in frequency by temperature and by piezo transducers. The frequency scanning rate by temperature tuning is limited in speed and in accuracy by the temperature controlling unit of the laser. The scanning by PZT is reproducible and scan rates of 1 GHz/ms could be achieved. The typical PZT tuning in this work is in steps of a few MHz in 100 ms to 1 s. The passive frequency stability of these lasers is very good if they are operated in a temperature stabilized environment. The frequency drift is less than 50 MHz/h and the day to day variation in the reproducibility is better than 500 MHz. They show a large hysteresis for PZT scanning in particular for large frequency scan rates. For a frequency step of 10 GHz this can amount up to about 100 MHz. Each of the laser systems has a second output, which can be used to monitor the wavelength on a wavelength meter WS6 (from High Finesse GmbH, Tübingen, Germany) and to perform further diagnostics. The power level of this monitor output is a few % of the main output power.

Diode Lasers

Visible laser light is generated with the laser diodes QLD-660-80S (from QPhotonics, VA, USA) and DL3149-057 (from Thorlabs. Inc., NJ, USA) at the wavelengths λ_2 and λ_3. For infra-red light at wavelength λ_{IR2} a laser diode LD-1120-0300-1 (from TOPTICA Photonics AG, Gräfelfing, Germany) is used. The

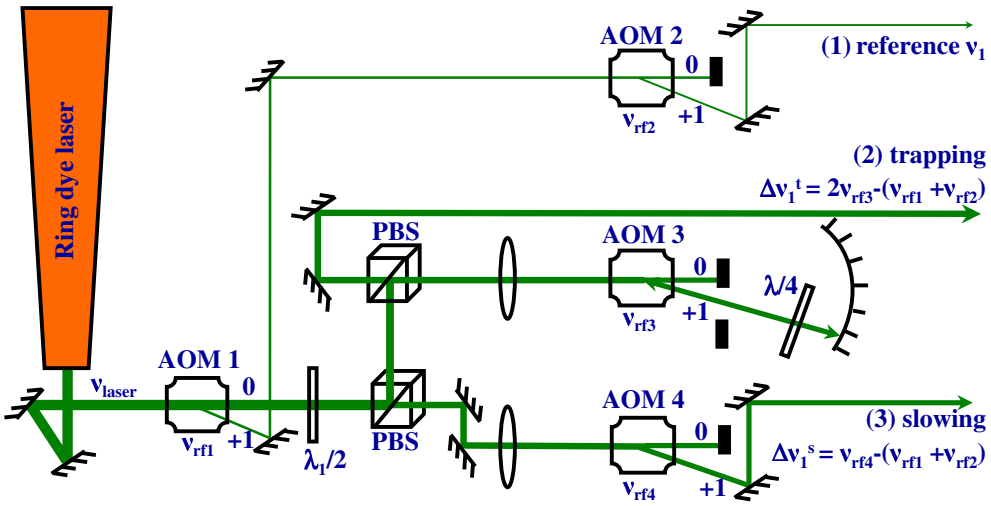

Fig. 4.2: Schematics for generating individual frequencies at wavelength λ_1. The frequencies can be tuned independently via the modulation frequencies of the acousto optic modulators AOM1, AOM2, AOM3 and AOM4. The reference beam at frequency ν_1 is for Doppler free spectroscopy of the $6s^2\ ^1S_0 \rightarrow 6s6p\ ^1P_1$ transition, the deceleration beam at frequency detuning $\Delta\nu_1^s$ is for slowing the atomic beam and the trapping beam at frequency detuning $\Delta\nu_1^t$ provides the light necessary for a MOT.

output powers are 8 mW, 5 mW and 250 mW respectively. The laser diodes are in commercially standardized packages of 5.6 mm and 9 mm diameter. They are stabilized in extended cavity diode laser configuration in home made mounting systems. The compact diode laser systems are user friendly for spectroscopy experiments because of their simplicity, size and cost [157,158]. Detailed descriptions of grating stabilized diode lasers can be found elsewhere [159,160].

A commercially available QFBLD-1550-20 distributed feedback diode laser (from QPhotonics, VA, USA) produced light at wavelength λ_{IR3} with a maximum output power of 17 mW. The frequency of this laser is stabilized with a grating within the semiconductor chip [160]. The light is coupled into a single mode fiber attached to the diode chip. The frequency can be changed by altering the laser's temperature or its operating current. The laser is tunable over a wide frequency range without any mode hops. A commercially available mount LM14S2 (from Thorlabs. Inc., NJ, USA) interfaces the laser in a 14 pin butterfly package to the temperature and the current controller.

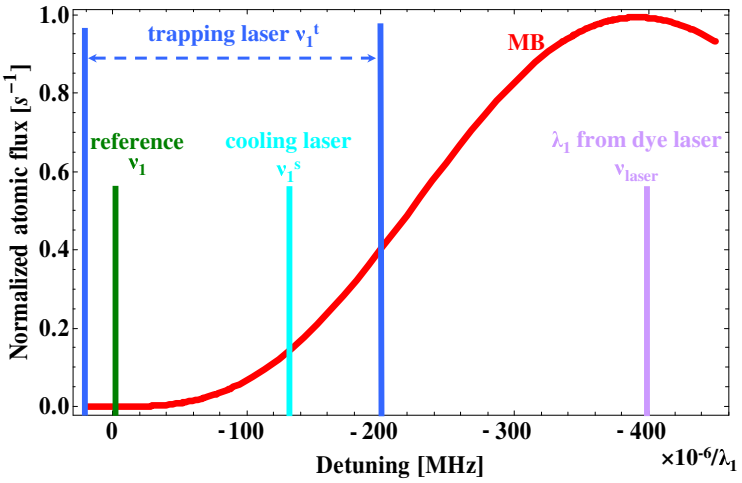

Fig. 4.3: Relative position of the laser frequencies for the three individual laser beams at wavelength λ_1. The Doppler shift of barium atoms with a Maxwell-Boltzman (MB) velocity distribution at 820 K temperature is shown to indicate the scale of the frequency intervals.

4.2.1 Multiple Frequency Generation

Multiple close lying laser frequencies are needed near the wavelengths λ_1, λ_{IR2} and λ_{IR3} to achieve both efficient cooling and trapping. For the two infrared wavelengths λ_{IR2} and λ_{IR3}, two lasers at each wavelength are used. The frequency offset of these pairs is controlled (see section 4.2.2).

Laser light at the dye laser wavelength λ_1 is employed at three slightly different frequencies. Acousto optical modulators (AOMs) can be used to generate these frequencies by modulating the light passing through them (see Figs. 4.2 and 4.3). In these devices (see Table 4.3) an integer multiple, m, of the modulation frequency, ν_{mod}, is added or subtracted from the laser frequency, ν_{laser}, to achieve the light frequency

$$\nu_{light} = \nu_{laser} \pm m \cdot \nu_{mod}. \tag{4.3}$$

Firstly, about 1 mW light is needed for the stabilization of the dye laser frequency to the resonance frequency, ν_1, of the $6s^2\ ^1S_0 \rightarrow 6s6p\ ^1P_1$ transition in ^{138}Ba. Secondly, the slowing of the atomic beam requires up to 30 mW power at a frequency detuning of $\Delta\nu_1^s$, which is typically -260 MHz from the atomic transition frequency ν_1. Thirdly, optical trapping requires about 30 mW power at a frequency detuning of $\Delta\nu_1^t$, which should be around ± 50 MHz. This light can also serve to probe the velocity distribution of atoms in the ground state $6s^2\ ^1S_0$. For this purpose the frequency detuning $\Delta\nu_1^t$ can be between -260 MHz

and 50 MHz at a power level of 1 mW.

The reference frequency ν_1 is generated by using the first (m = +1) order of AOM1, which is a model AOM-60 (from IntraAction Corp., IL, USA) and the first (m = +1) order of AOM2, which is a model MT-350-AO (from AA-OPTO-ELECTRONIC, Saint Remy Les Chevreuses, France). The light frequency is then

$$\nu_1 = \nu_{\text{laser}} + (\nu_{\text{rf1}} + \nu_{\text{rf2}}), \tag{4.4}$$

where ν_{rf1} and ν_{rf2} are the modulation frequencies to drive the AOMs. AOM1 diffracts about 2% of the dye laser output power and more than 1 mW of light is obtained at the frequency ν_1. The operating frequencies are $\nu_{\text{rf1}} = 60$ MHz and ν_{rf2} varies between 300 MHz and 500 MHz.

The undiffracted beam of AOM1 is split by a combination of a $\lambda/2$ wave-plate and a polarizing beam splitter cube. This allows to change the splitting ratio by rotating the polarization with the $\lambda/2$ wave-plate. One beam is used to generate the frequency detuning $\Delta\nu_1^{\text{t}}$ by double passing AOM3, which is a model TH-200-50 (from BRIMOSE Corp., MD, USA). The frequency detuning of the double pass first (m = +1) order beam is

$$\Delta\nu_1^{\text{t}} = 2 \cdot \nu_{\text{rf3}} - (\nu_{\text{rf1}} + \nu_{\text{rf2}}), \tag{4.5}$$

where ν_{rf3} is the operating frequency of AOM3. The double passing has an efficiency of about 30% at a frequency $\nu_{\text{rf3}} = 200$ MHz. More than 30 mW of light can be generated with the necessary frequency detuning for trapping. For measuring the velocity distribution of atoms in the ground state, ν_{rf3} is tuned between 130 MHz and 280 MHz to cover the low velocity range of the spectrum. The laser light after double passing is power stabilized to better than 1% at around 1 mW over the entire tuning range.

The second beam from the polarizing beam splitter cube is used to generate the frequency detuning $\Delta\nu_1^{\text{s}}$, which is the first (m = +1) order diffracted beam of AOM4. It is a model TH-200-50 (from BRIMOSE Corp., MD, USA) operating at a radio frequency, ν_{rf4}, which yields

$$\Delta\nu_1^{\text{s}} = \nu_{\text{rf4}} - (\nu_{\text{rf1}} + \nu_{\text{rf2}}). \tag{4.6}$$

This light is used for deceleration of the atomic beam. The frequency ν_{rf4} can be tuned from 160 MHz to 260 MHz while more than 30 mW of light can be obtained.

The AOM's in this setup can also be used for fast switching of the light power in the different laser beams. The switching time for the light was faster than

	AOM1	AOM2	AOM3	AOM4
Part No. Supplier	AOM-60 IntraAction Corp., USA	MT-350-AO, AA-OPTO-ELECTRONIC, France	TH-200-50 BRIMOSE Corp., USA	TH-200-50 BRIMOSE Corp., USA
Modulation frequency [MHz]	60	$300 - 500$	$130 - 280$	$160 - 260$
Purpose	active beam splitter	frequency stabilization ν_1	trapping laser detuning $\Delta\nu_1^{\mathrm{t}}$	slowing laser detuning $\Delta\nu_1^{\mathrm{s}}$

Table 4.3: The relevant frequencies and power ratios can be controlled easily by the modulation frequencies and the power applied to the four AOM's.

1 μs. The power, frequency detuning and the time structure of the three laser beams near wavelength λ_1 can be controlled independently by this setup.

4.2.2 Stabilization of the Lasers

Power stabilization can be implemented for all laser beams behind one of the AOM's. The diffracted power is monitored on a photodiode. An error signal is generated by subtracting a set point voltage from the photodiode signal voltage. This error signal is fed into a phase detector, which acts as a variable attenuator for the rf power which drives the AOM. Only the trapping laser beams are power stabilized rather than the output of the dye laser. The dye laser output has power fluctuations within $3 - 4\%$. This is reduced to below 1% with stabilization. The power stabilization of the light is essential for probing the velocity distribution in the atomic beam. The output power of the fiber lasers and the diode lasers are stable to better than 0.5% and need no further stabilization.

The distributed feedback diode laser at wavelength λ_{IR3} drifts far less in its frequency (< 10 MHz/h) than the fiber lasers in a temperature controlled environment. The frequency offset for each pair of lasers at the wavelengths λ_{IR2} and λ_{IR3} is stabilized. At wavelength λ_{IR2} the laser frequency is locked to the frequency of the fiber laser. At wavelength λ_{IR3} the frequency of the fiber laser is stabilized to the diode laser frequency. For each laser pair about 150-200 μW of light is split off. The resulting beams are overlapped on a beam splitter (see Fig.

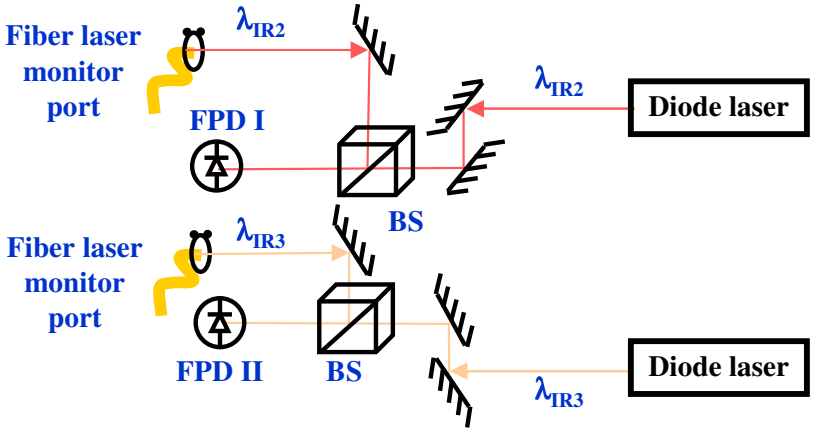

Fig. 4.4: Schematics for generating beat notes at the wavelengths λ_{IR2} and λ_{IR3}.

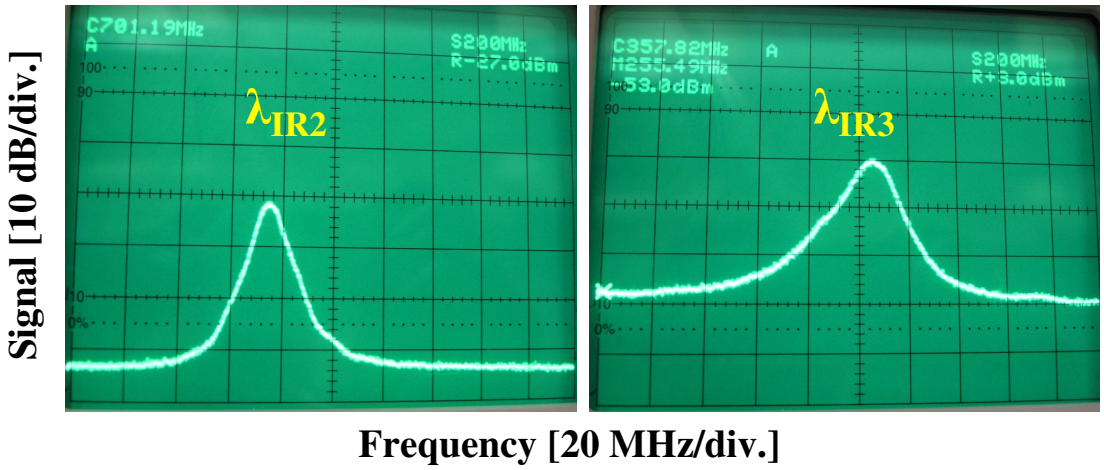

Fig. 4.5: Photographs of the typical beat note signals between two laser beam pairs at the wavelengths λ_{IR2} and λ_{IR3}. The estimated width of the beat note spectrum at wavelength λ_{IR2} is 18(2) MHz and at wavelength λ_{IR3} it is 24(2) MHz. The signal-to-noise ratio (S/N) is about 30 dB with 1 MHz resolution bandwidth.

	λ_{IR3}	λ_{IR2}
Signal amplitude	−68 dBm	−27 dBm
PD output across 50 Ω	3.5 mV	8.7 mV
FWHM of typical spectrum	35(5) MHz	20(5) MHz

Table 4.4: General characteristics of the beat notes at the wavelengths λ_{IR3} and λ_{IR2}.

4.4). The combined beams are focussed onto a fast FGA04 InGaAs photodiode (from Thorlabs Inc., NJ, USA) to detect the beat note signal (see Fig. 4.5). The beat note signal depends on the intensities, I_a and I_b, of the two laser beams, the angle, ϕ, between the directions of polarization of both beams, the frequency offset, $\Delta\nu_{BN}$, between the two lasers and the angle, θ, between the two beams. The intensity of the two superimposed co-propagating beams at $\theta = 0^o$ is

$$I(t) = (I_a + I_b) + 2\sqrt{I_a\, I_b} \cdot \cos\phi \cdot \cos\left(2\pi\, \Delta\nu_{BN}\, t\right), \tag{4.7}$$

where t is the time [162]. The photodiode detects the time dependent intensity I(t). At parallel polarization of the two laser beams the ac part of the photodiode signal carries information only about the frequency difference $\Delta\nu_{BN}$, i.e., the beat note. The typical parameters of the radio frequency (rf) signal from these diodes are given in Table 4.4. The signals are amplified and split into two parts each. One is fed into a frequency counter which can be read by the data acquisition system. The other part can be exploited for frequency offset locking [161]. For this, the signal $\Delta\nu_{BN}$ is feed to a phase locked loop (PLL) circuit on a ADF4007 evaluation board (from Analog Devices Inc., MA, USA). The frequency offset between $\Delta\nu_{BN}$ and a reference frequency is converted by the ADF4007 evaluation board into a voltage which is proportional to the frequency deviation. This signal can be used as an error signal as an input to a PID controller. The control voltage is fed to one of the lasers to keep the frequency difference $\Delta\nu_{BN}$ constant [163].

4.2.3 Optics Layout

The interaction of the atoms with laser beams at the different wavelengths is achieved by spatial overlapping of the individual laser beams (see Fig. 4.6). This is done for several combinations of laser wavelengths. Each pair of infrared laser beams at the wavelengths λ_{IR2} and λ_{IR3} is combined with a high efficiency dichroic mirror PRA-1500-90-1037/BBAR-1050-1600 (from CVI Laser Optics, NM, USA)

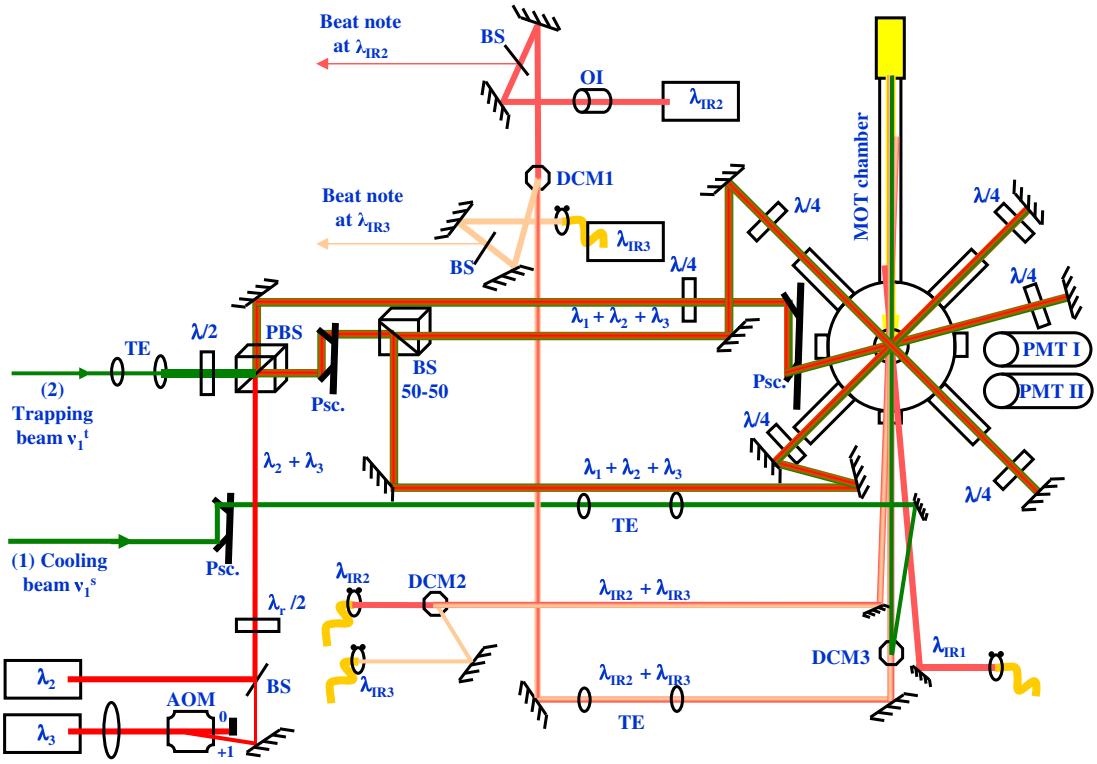

Fig. 4.6: Optics arrangement for overlapping nine laser beams of different frequencies. AOM - acousto optic modulator, BS - beam splitter, DCM - dichroic mirror, FPD - fast photodiode, $\lambda/2$ and $\lambda_r/2$ - half wave plates, $\lambda/4$ - quarter wave plate, OI - optical isolator, PBS - polarizing beam splitter, PD - photodiode, Psc. - periscope, PMT - photomultiplier tube, TE - telescope. The drawing is not to scale.

(see Fig. 4.6). These beam splitters are coated such that 75 % of the power at wavelength λ_{IR3} is reflected and 85 % of the power at wavelength λ_{IR2} is transmitted for small incidence angles. The combined laser beams from DCM1 are overlapped with the slowing laser beam at wavelength λ_1 on an another dichroic mirror PRA-532-98-1037/BBAR-1050-1600 (from CVI laser optics, MN, USA). It reflects 85% at wavelength λ_1 and transmits 80% of the power at the wavelengths λ_{IR2} and λ_{IR3}. Two telescopes provide for changing the beam diameters and divergences independently.

The laser beams at wavelength λ_{IR1} and the combined laser beams at the wavelengths λ_{IR2} and λ_{IR3} are brought into the vacuum chamber at a shallow angle with respect to the slowing laser beam. The laser beams at the wavelengths λ_2 and λ_3 are combined on a beam splitter and are overlapped with the trapping laser beam on a polarizing beam splitter cube. The alignment of all laser beams

relative to each other is crucial for the performance of such experiments, where multiple atomic transitions are involved. The tolerance for overlapping all the laser beams is about 0.5 mm, which is about 1/3 of the trapped cloud diameter.

The vacuum chamber, all lasers and all the optics are mounted on a honeycomb structured optics table (from Newport Corp., CA, USA) with pneumatic damping to isolate the setup from mechanical vibrations. The volume above the table is enclosed by plastic curtains and a continuous laminar air flow from the top cover protects the setup from dust.

4.3 Fluorescence Detection

The fluorescence from the atomic beam or from trapped atoms can be detected by two R7205-01 (from Hammamatsu Corp., Shizuoka, Japan) photomultiplier tubes. Narrow band interference filters FB410-10 or FB550-10 (from Thorlabs Inc., NJ, USA) are mounted in front of the photomultipliers to select the fluorescence at the wavelengths λ_B or λ_1. Both photomultipliers have the same field of view.

The imaging system (see Fig. 4.7) consists of a plano-convex lens of focal length f = 60 mm, mounted close to an optical vacuum window (see Fig. 4.1). The lens is at a distance of 135(5) mm from the trap center and collects fluorescence with a solid angle $\Omega = 4.2 \cdot 10^{-3}$ sr. An aperture is placed at the position of the image plane 155(5) mm downstream of the collection lens. The magnification of the imaging system is 1.20(7). The light transmitted through the aperture is collimated by a lens of focal length f = 30 mm at 30 mm distance from the image O′. A beam splitter is used to illuminate both photomultipliers simultaneously.

The detection efficiency, ϵ_i, at a particular wavelength, λ_i (i = 1, B), depends on the solid angle, Ω, for the light collection, the splitting fraction $\epsilon_{BS} = 1 : 2.4$ of the beam splitter in front of the photomultipliers, the transmission, ϵ_f, through the interference filters and the quantum efficiency of the photomultiplier cathode, $\varepsilon_i(\lambda_i)$, at the wavelength λ_i

$$\epsilon_i = \Omega \cdot \epsilon_{BS} \cdot \epsilon_f \cdot \varepsilon_i(\lambda_i). \tag{4.8}$$

The transmission of both interference filters is $\epsilon_f = 52(2)$ %. In most of the measurements PMT-I was used with a filter transmitting wavelength λ_B, which gives an efficiency of $\epsilon_B = 8(1) \cdot 10^{-5}$ and PMT-II with a filter for wavelength λ_1 resulting in an efficiency of $\epsilon_1 = 10(1) \cdot 10^{-5}$.

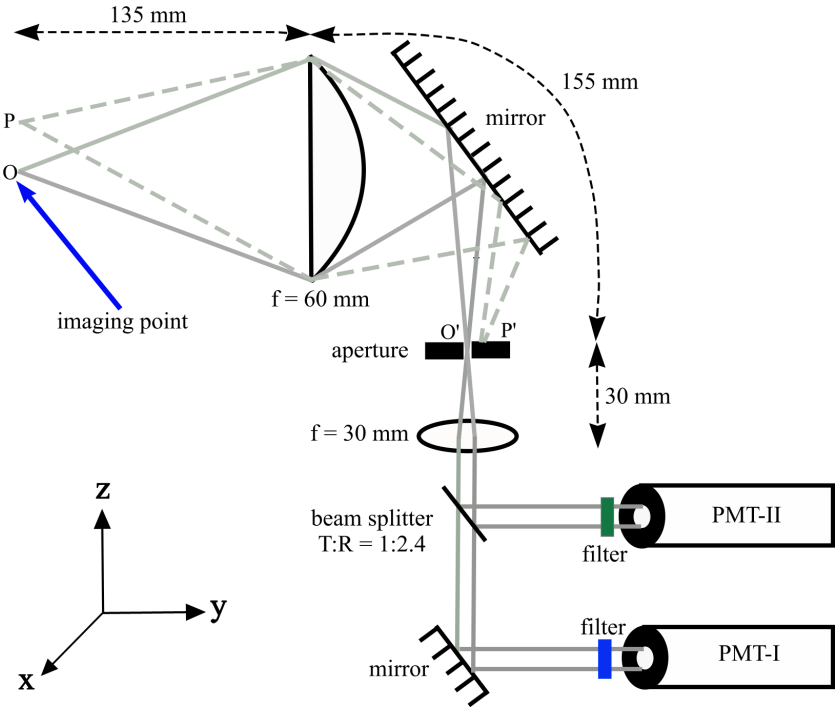

Fig. 4.7: Schematics of the optics arrangement for imaging the fluorescence signal onto the photomultiplier photocathodes. The magnification of the imaging system is 1.20(7). The beam splitter transmits about 30% and reflects about 70% of the collected fluorescence light. The imaging volume can be changed by changing the size of the aperture.

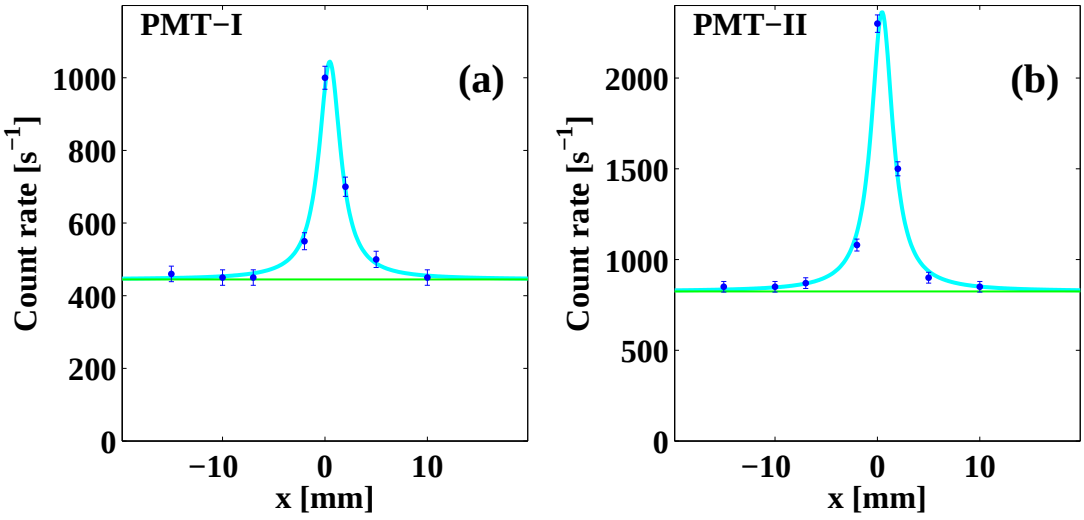

Fig. 4.8: Spatial acceptance of fluorescence with an aperture size of 2 mm. The fitted width to the spectra is 2.5(2) mm and the signal ratio in PMT-I and PMT-II is 1 : 2.4(2). The horizontal line corresponds to scattered background photons.

The relative efficiencies and the field of view for the two photomultipliers were verified with the fluorescence signal from the atomic beam. A weak probe beam at wavelength λ_1 along the z-axis intersected the atomic beam orthogonally. The position of the probe beam was moved in the x-direction, i.e., along the atomic beam direction of propagation, while the fluorescence at wavelength λ_1 was detected on both photomultipliers simultaneously without filters in front of the PMT's. The count rate ratio was $1 : 2.4(2)$ and the width of the signal was 2.5(2) mm (see Fig. 4.8). Both figures agree well with the design values of the imaging system.

4.4 Data Acquisition

The control of the laser frequencies, the readout of the photomultiplier rates and the beat note frequencies is based on GPIB (General Purpose Interface Bus) devices, which are connected via a 488-USB interface (from ICS Electronics, CA, USA) to a personal computer. The scan parameters can be selected and the spectra can be stored for further analysis with a control programme written in C++. The schematics of the control devices and the readout setup are given in Fig. 4.9. Four frequency counters read the beat note frequencies and the count rates from the photomultiplier tubes. All lasers can be set and scanned in their frequencies with 8 analog voltages from a DAC (Digital to Analog Converter) device SR-245 (from Stanford Research Systems Inc., Palo Alto, USA).

4.5 Magnetic Field

The quadrupole magnetic field is generated by a pair of coils with identical dimensions separated by a distance (for dimensions see Table 4.5). Both coils carry a current in opposite relative direction (close to anti-Helmholtz configuration). The coils are made from copper wire of 2 mm diameter wound onto aluminium frames. The coils are mounted outside the vacuum chamber along the z-axis and orthogonal to the atomic beam (see Fig. 4.10). The power dissipation at their maximum current of 20 A is about 350 W. The coils are air cooled by a fan unit.

The calculated field gradients produced by the coils along the z-axis and in the radial directions (xy-plane) are $\alpha_z = 1.85(5)$ G cm^{-1}A^{-1} and $\alpha_{x,y} = 0.88(2)$ G cm^{-1} A^{-1} within the trapping volume (see Figs. 4.11 and 4.12). In the MOT, the magnetic field is important only within the trapping volume defined by the

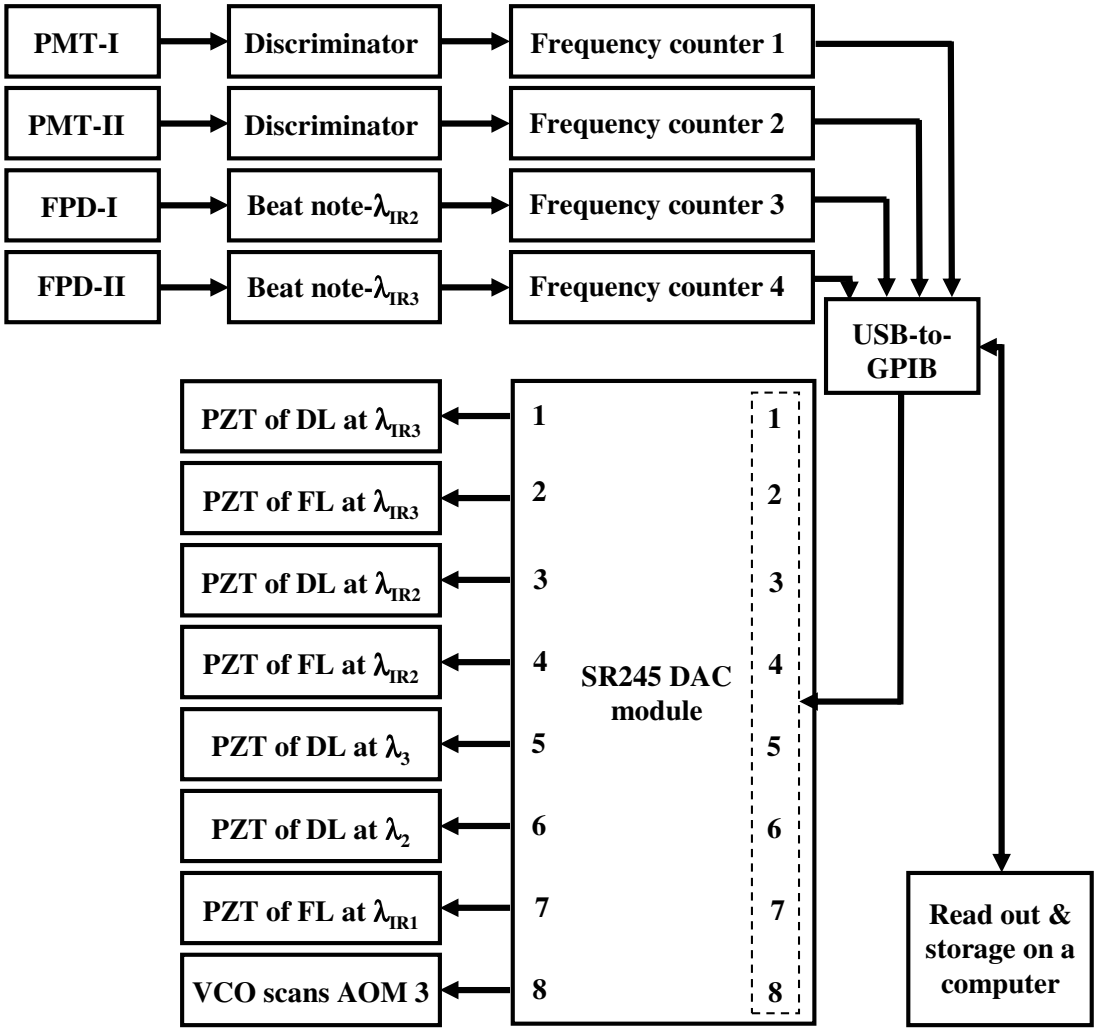

Fig. 4.9: Block diagram of the control and data acquisition system. Four frequency counters count the discriminator pulse rates and offset frequencies of the laser pairs at wavelength λ_{IR2} and λ_{IR3} measured via beat notes. The lasers can be scanned with voltage from Digital to Analog Converter channels connected to the laser analog scan inputs. An USB-to-GPIB interface connects the counters and DAC to a personal computer.

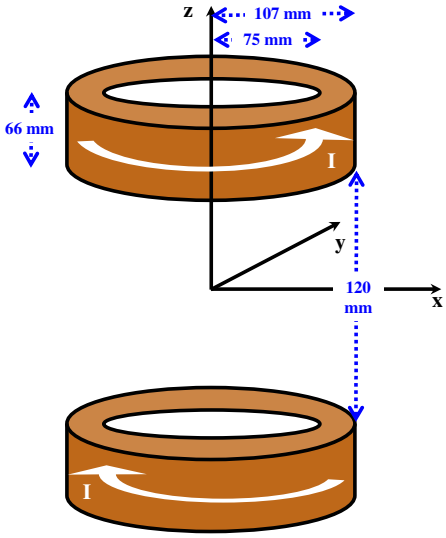

Fig. 4.10: Schematics of the coils, which produce a quadrupole magnetic field. The axis of the coils is defined as the z-direction, the atomic beam is propagating along the x-direction. The dimensions of the coils are indicated. The drawing is not to scale.

diameters of the laser beams.

The numerical magnetic field calculation for the coils arranged close to Helmholtz configuration (see Appendix A) was compared with the measured Zeeman splitting of the $6s^2\ {}^1S_0 \rightarrow 6s6p\ {}^1P_1$ transition at wavelength λ_1. The ground state $6s^2\ {}^1S_0$ has no Zeeman splitting and the excited state $6s6p\ {}^1P_1$ has three magnetic sub-levels $m_j = 0, \pm 1$ with the g-factors $g_j = 1$. With excitation transverse to the field and along the magnetic field axis the fluorescence was detected radially along the y-direction. This selects only σ^+ ($\Delta m_j = +1$) and σ^- ($\Delta m_j = -1$) transitions (see Fig. 4.13 a). At a constant magnetic field B the splitting between the σ^+ and the σ^- transitions is

$$\Delta\nu(B) = 2 \cdot \frac{\mu_B\ B}{h}. \tag{4.9}$$

The splitting, $\Delta\nu(B)$, for different values of the magnetic field was measured. A linear function can be fitted to the measurements. An offset of 1.3(7) G arises due to magnetization of the table and environmental stray fields. The calibration constant of the coils is 6.37(6) G/A (see Fig. 4.13 b) which is in good agreement with the calculated value of 6.6(2) G/A. The uncertainty of the calculation arises from the mechanical tolerances of the coils.

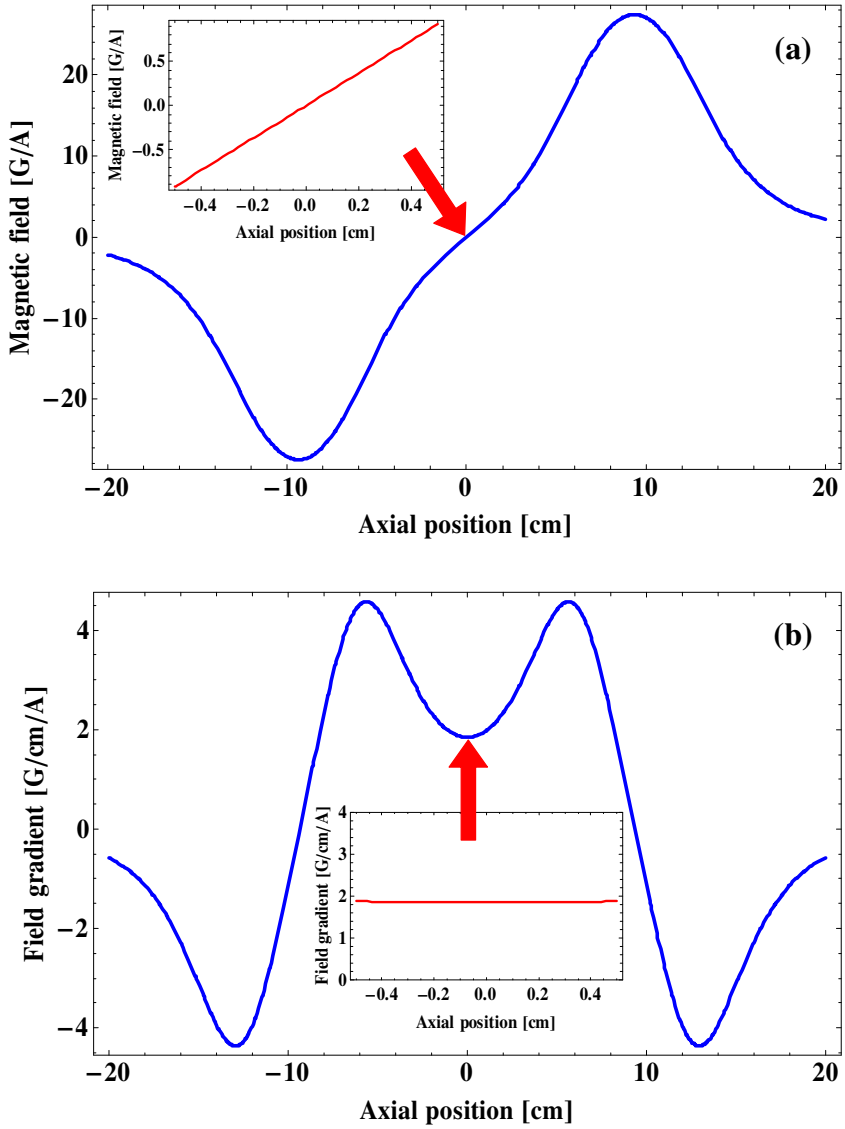

Fig. 4.11: (a) Magnetic field and (b) magnetic field gradient per unit current for the MOT coils. The inset is the typical region where trapping occurs.

Inner radius R_i	75(1) mm
Outer radius R_o	107(2) mm
Axial separation between two close end of the coils L	120.0(5) mm
Height of coils h	66(1) mm
Number of turns in each coils N	215
Diameter of copper wire Φ	2 mm
Resistance of each coil	0.42(2) Ω
Dumped power in total	150 W

Table 4.5: Specification of the MOT coils producing a quadrupole magnetic field for the experiments. Both coils are identical in geometry and wired in anti-Helmholtz configuration.

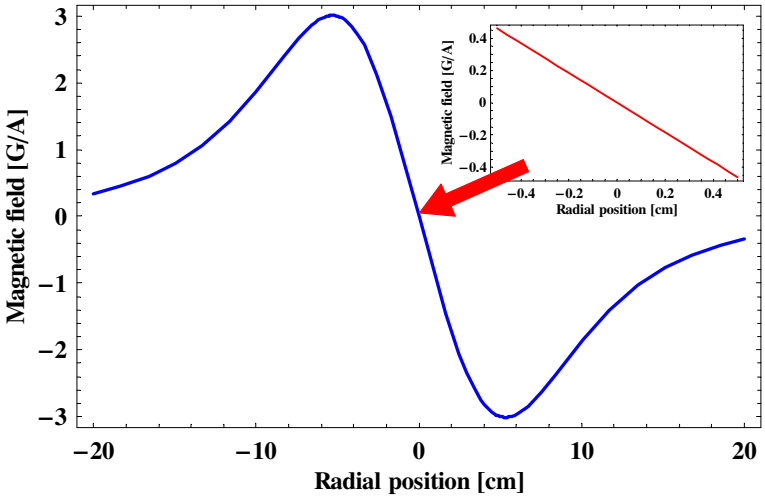

Fig. 4.12: Magnetic field produced by the MOT coils along the radial directions, i.e., in the xy-plane. The inset is the typical region where trapping occurs.

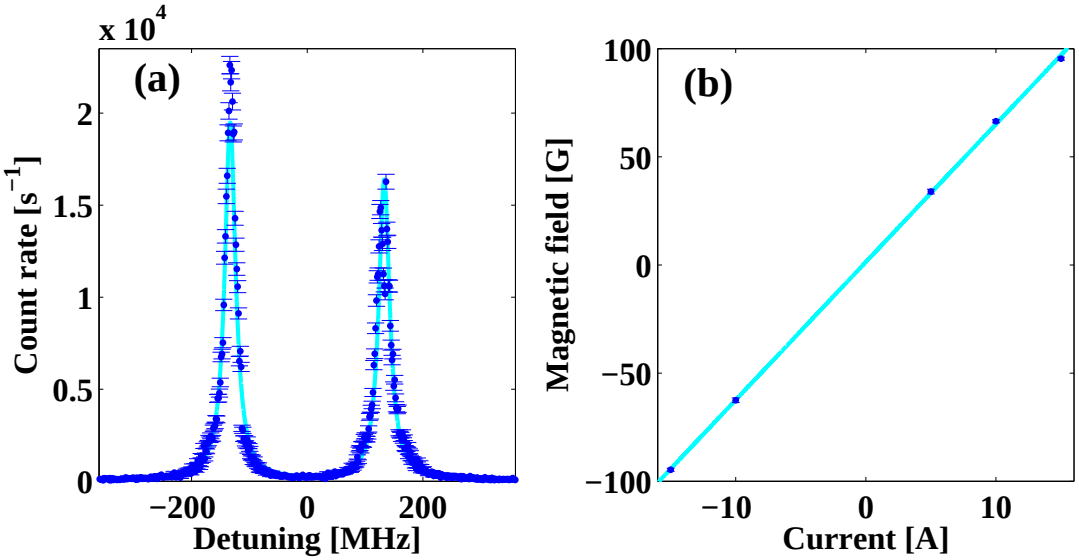

Fig. 4.13: Measured (a) Zeeman splitting of the $6s^2\ ^1S_0 \rightarrow 6s6p\ ^1P_1$ transition of ^{138}Ba in a homogenous magnetic field. The different peak heights of the σ^+ and the σ^- transitions are due to the spatial acceptance of the PMT. The two resonance appear spatially not symmetric with respect to the detection axis, because of the field offset. The splitting of the lines is 267(2) MHz at a current of 15 A in the coils. (b) Magnetic field according to the Zeeman splitting measurements at various coil currents. The line fitted to the measured data gives a magnetic field calibration of B = 6.37(6) G/A with an offset B_o = 1.3(7) G from environmental background.